RSC Advances

PAPER

View Article Online
View Journal | View Issue

Check for updates

Cite this: *RSC Adv.*, 2020, **10**, 29510

Manifold of self-assembly of a *de novo* designed peptide: amyloid fibrils, peptide bundles, and fractals†

Yu-Jo Chao,‡ Kan Wu,‡ Hsun-Hui Chang, Ming-Jou Chien and Jerry Chun Chung Chan *

Received 20th May 2020
Accepted 2nd August 2020

DOI: 10.1039/d0ra04480f

rsc.li/rsc-advances

We report that a peptide with the sequence of EGAGAAAAGAGE can have different aggregation states, *viz.*, amyloid fibrils, peptide bundles, and fractal assembly under different incubation conditions. The chemical state of the Glu residue played a pivotal regulating role in the aggregation behavior of the peptide. The mechanism of the fractal assembly of this peptide has been unraveled as follows. The peptide fragments adopting the beta-sheet conformation are well dispersed in alkaline solution. In the buffer of sodium bicarbonate, peptide rods are formed with considerable structural rigidity at the C- and N-termini. The peptide rods undergo random trajectory in the solution and form a fractal pattern on a two-dimensional surface *via* the diffusion-limited aggregation process.

Introduction

Scale invariant structures are called fractals.[1] Fractal structures refer to patterns exhibiting self-similarity over multiple length scales, which are ubiquitously found in natural systems such as coastlines, snowflakes, neuron network, and bacterial colonies.[2] Because a fractal object scales by a non-integer (fractal) dimensionality, the high surface-to-volume ratio of fractal assemblies have been actively exploited by Nature for various biological functions.[1] Fabrications of fractal assembly have been conducted for a large variety of materials such as inorganic metal–ligand complexes,[3–6] aromatic bromo compounds,[7] DNA origami tiles,[8] proteins,[9–11] block copolymers,[12] conjugated polymers,[13] and liquid crystal colloids.[14] Very recently, it has been shown that the fractal assemblies of engineered proteins could exhibit biomimetic functionality, which has aptly illustrated the vast potential of the bottom-up design of fractal topologies for the development of functional biomaterials.[15,16] Biomolecules such as lysozyme,[17] coiled-coil peptides,[18,19] peptide derivatives,[20,21] and polyalanine peptides[22] could form fractal assemblies but a detailed understanding of the structural features of the protein building blocks remains largely elusive.

To develop a stimulus-responsive fractal assembly of peptide, the first consideration is to choose the mechanism for the self-assembly of the peptide building blocks. In this regard, we notice that a structural motif of amyloid fibrils, *viz.* steric zipper, has a strong propensity to aggregate, for which the residues of two neighboring beta-sheet layers are tightly interdigitated.[23] In particular, the steric zippers formed by the polypeptides containing the sequence of AGAAAAGA have multiple β-sheet layers closely stacked together.[24] For convenience, this palindromic sequence is referred to as alanine steric zipper (ASZ) in our subsequent discussion. Hydrophobic interaction alone usually would lead to the formation of random aggregates in aqueous solution. Thus, we hypothesized that one may attenuate the aggregation propensity of a steric zipper by adding acidic or basic residues to its peptide chain. One legitimate design is to attach an acidic residue such as Glu to both the C- and N-termini of ASZ, with Gly residues inserted in between. The resultant polypeptide with the sequence of Ac-EGAGAAAAGAGE-NH_2 is henceforth referred to as EASZ. In this work, we report that the EASZ peptides could form fractal assembly on a two-dimensional (2D) surface under chemically controlled conditions and the peptides adopted the cross-β motif commonly found in amyloid fibrils.[25]

Materials and method

Peptide synthesis

Isotopically enriched (^{13}C and ^{15}N) amino acids with 9-fluorenylmethoxycarbonyl (FMOC) protection were obtained from Cambridge Isotope Laboratories (Andover, MA), CortecNet (Tilleuls, France), and Isotec (St. Louis, MO). Unlabeled FMOC-amino acids were obtained from NovaBiochem and other chemicals from Acros unless stated otherwise. The EASZ peptides, with the sequence Ac-EGAGAAAAGAGE-NH_2, were synthesized on an automated Odyssey microwave peptide

Department of Chemistry, National Taiwan University, No. 1, Section 4, Roosevelt Road, Taipei, 10617, Taiwan. E-mail: chanjcc@ntu.edu.tw

† Electronic supplementary information (ESI) available. See DOI: 10.1039/d0ra04480f

‡ Authors contributed equally.

Open Access Article. Published on 10 August 2020. Downloaded on 2/1/2026 3:57:00 AM. This article is licensed under a Creative Commons Attribution-NonCommercial 3.0 Unported Licence.

This journal is © The Royal Society of Chemistry 2020

Open Access Article. Published on 10 August 2020. Downloaded on 2/1/2026 3:57:00 AM.
This article is licensed under a Creative Commons Attribution-NonCommercial 3.0 Unported Licence.

synthesizer (CEM Corp., Matthews, NC), using Rink amide resin (Novabiochem) and FMOC chemistry. The synthesis scale was 0.1 mmol, with a 2-fold and 5-fold excess for isotopically labeled and unlabeled amino acid, respectively. The coupling step was carried out for 5 min at 75 °C. Crude peptides were cleaved from the synthesis resin using standard protocols (reaction for 105 min in 95% trifluoroacetic acid (TFA) and 5% triisopropyl silane), which were then precipitated in cold methyl *tert*-butyl ether (MTBE). Precipitated peptides were washed three times with cold MTBE and then lyophilized. The crude material was purified by high-performance liquid chromatography at room temperature, using a water/acetonitrile gradient with 0.1% TFA and a Vydac C18 reverse-phase column of preparative scale. Samples of 5 mg per injection were dissolved in 50 μL of TFA and then diluted to 5 mL with 8% acetonitrile in DI water before being injected into the column. Fractions containing the target product were frozen in liquid nitrogen and lyophilized immediately after being collected.

Gas diffusion experiment

The peptides (1–1.5 mM) were incubated under acidic condition (pH 2.0, 5 mM $CaCl_2$) for 8 hours, using $HCl_{(aq)}$ for pH adjustment unless stated otherwise. For the gas diffusion experiment, 100 μL of the peptide solution was dropped on parafilm and placed in a closed desiccator with a glass vial of 1 g of $(NH_4)_2CO_{3(s)}$.

Sample characterization

The measurements of zeta potential and dynamic light scattering (DLS) were carried out using a commercial instrument (Malvern Zetasizer ZS300). Transmittance FT-IR spectra were collected using a Magna-IR 550 spectrometer (series II), in the range of 1000–4000 cm^{-1}.

Electron microscopy

Scanning Electron Microscopy (SEM) images were taken on a JEOL JSM-7600F field emission scanning electron microscope operated at 10 kV. The samples were dispersed on a carbon tape mounted on a metal holder, followed by coating a layer of platinum with low-vacuum sputtering at 10 mA for 90 s. Transmission Electron Microscopy (TEM) images were acquired on a Hitachi H7100 field emission electron microscope operated at 75 kV.

Solid-state NMR

All NMR experiments were carried out at ^{13}C and ^{1}H resonance frequencies of 100.62 and 400.15 MHz, respectively, on a Bruker Avance III spectrometer equipped with a commercial 2.5 mm probe. Samples were confined in the middle of the rotor volume using Teflon spacers to enhance the RF homogeneity. ^{13}C and ^{1}H chemical shifts were externally referenced to tetramethylsilane, using adamantane as the secondary reference. For the $^{13}C\{^{1}H\}$ cross-polarization magic-angle spinning (CPMAS) experiments[26] at a spinning frequency of 18 kHz, the ^{1}H nutation frequency was set to 50 kHz and that of ^{13}C was ramped through the Hartmann–Hahn condition linearly.[27] Two Pulse Phase Modulation (TPPM)[28] proton decoupling of 70 kHz was applied during the acquisition period. For the ^{13}C–^{13}C dipolar-assisted rotational resonance (DARR) correlation spectroscopy,[29,30] the mixing period was set to 150 ms with the ^{1}H nutation frequency equal to 18 kHz. The durations of all ^{1}H and ^{13}C $\pi/2$ pulses were set to be 5 μs. Two Pulse Phase Modulation (TPPM) proton decoupling[28] of 70 kHz was applied during both the mixing and acquisition periods. The recycle delay was 3 s. The t_1 quadrature detection was achieved using the States-TPPI scheme.[31] A total of 256 increments was acquired at steps of 33.3 μs. The spectral deconvolution of the $^{13}C\{^{1}H\}$ CPMAS spectra were carried out using DMFit2011.[32]

Results and discussion

Fibrillar aggregates of EASZ peptides

The target palindromic peptide sequence EASZ was prepared by solid-phase peptide synthesis. After incubating the peptide solution (0.2 mM) at pH 2.0 for eight hours, the solution became cloudy. Thioflavin-T (ThT) fluorescence assay and infrared spectroscopy are well suited to detect the presence of β-sheet-rich peptide assembly (Fig. S1 and S2†).[33,34] In the TEM image for the peptide sample, fibrillar aggregates of length in the range of 120 to 320 nm and the width from 7 to 18 nm were observed (Fig. 1a and S3†). Altogether we unequivocally showed that the peptides under acidic conditions formed amyloid fibrils, adopting the cross-β structural motif. When the pH of the peptide solution was increased to 9.0 by dialysis against $NaOH_{(aq)}$, the solution became clear. That is, the amyloid fibrils were soluble at high pH. This observation is not unexpected

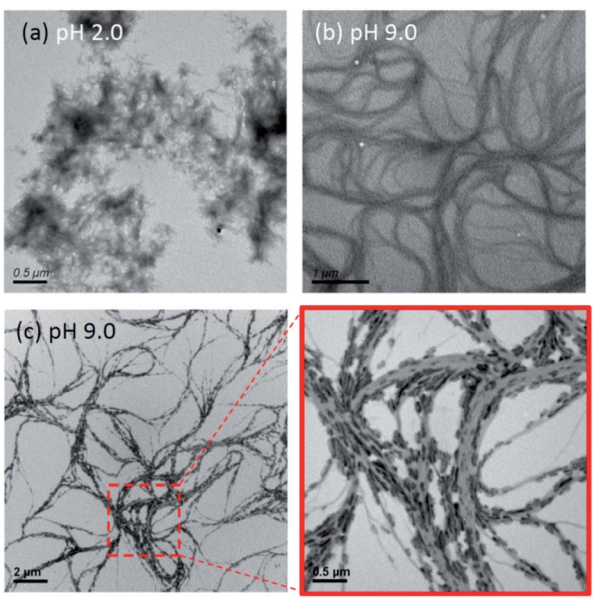

Fig. 1 Unstained TEM images of the EASZ peptides at different aggregation states. (a) Amyloid fibrils formed at pH 2.0. (b) Spaghetti-like peptide bundles formed at pH 9.0. (c) Peptide bundles after aging under the atmosphere of NH_3 and CO_2. The inset shows the formation of mineral salt on the peptide bundles.

Open Access Article. Published on 10 August 2020. Downloaded on 2/1/2026 3:57:00 AM.
This article is licensed under a Creative Commons Attribution-NonCommercial 3.0 Unported Licence.

because the deprotonation of the Glu residues at high pH should disrupt the peptide aggregates. The zeta potentials of the peptide aggregates at pH 2.0 and 7.0 were determined to be −1.04 and −50.2 mV, respectively. The highly negative zeta potential accounted well for the stability of the peptide aggregates against precipitation under alkaline conditions.

The transmission electron microscopy (TEM) images acquired at pH 9.0 (Fig. 1b) showed that the peptides assembled into spaghetti-like bundles over a length scale of many microns and the morphology was drastically different from that of amyloid fibrils. This pH-dependent phenomenon is commonly observed in protein assembly.[9,11] It is not trivial to determine whether the bundle formation was triggered when the peptide solution was dispersed on the copper grid for TEM measurements. To address this issue, we attempted to induce mineral formation on the peptide aggregates by gas diffusion experiment, where the peptide solution was incubated under an atmosphere of ammonia and carbon dioxide for an hour. As shown in Fig. 1c, nano-sized crystallites were deposited as "dashed lines" along the peptide bundles. Additional experiments indicated that the minerals deposited were ammonium salts (see Fig. S4†). This phenomenon confirmed that the peptide bundles were present in the bulk solution. A more careful scrutiny revealed that: (i) the crystallites were rather uniform in length (∼200 nm) and width (∼30 nm); (ii) the orientation of each crystallite was closely aligned to the tangent vector of the curvy bundles; (iii) the peptide bundles have a much longer length scale than the amyloid-fibril counterpart. These observations implied that the crystallites of the ammonium salt were formed epitaxially on the charged arrays of the peptide bundles and that the long axis of the discrete charge arrays of Glu paralleled the propagation direction of the peptide bundles.

Fractal pattern formed by EASZ peptides

Very recently, it has been suggested that salt may act as a mediator for the fractal assembly of human amylin[11] and peptide bundlemer chains.[35] Because well dispersed peptide bundles instead of random aggregates were formed at high pH, the long-range interaction mediated by the attraction force between Na^+ ions and the COO^- groups of Glu was presumably anisotropic. We surmised that if such long-range ionic interaction was screened out, a free peptide building block may undergo a random-walk trajectory before attaching to an existing cluster, leading to the formation of stochastic fractals.[36] To test this idea, the peptide solution at pH 9.0 was dialyzed against sodium bicarbonate buffer (20 mM, pH 9.0) for one hour. Remarkably, dendritic patterns were found in the TEM images (Fig. 2a and b), which is in stark contrast to the spaghetti-like bundles before the dialysis. The pattern exhibited the features of randomly branching and appeared to be stochastically self-similar. The same result was also observed in the scanning electron microscopy (SEM) images (Fig. 2c and d), for which the peptide solution was dried on a silicon wafer. For comparison, the peptide solution was lyophilized and studied by SEM. As shown in Fig. S5,† only random aggregates of nanorods were observed in the absence of a 2D substrate. The size of the nanorods were comparable to that of the amyloid fibrils formed under acidic conditions. Measurements of dynamic light scattering confirmed that nanoaggregates were indeed present in the peptide solution (Fig. S6†). Thus, we inferred that the dendritic pattern of the peptide nanorods shown in Fig. 2c was induced by drying on a 2D surface.

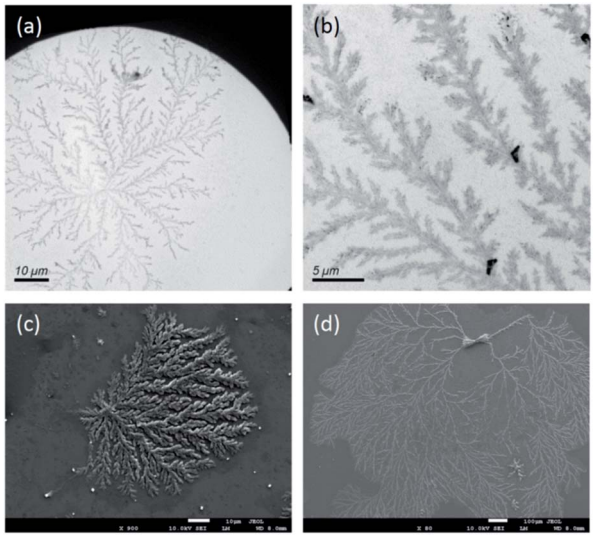

Fig. 2 TEM (a and b) and SEM (c and d) images of the fractal assembly formed by the EASZ peptides after dialysis in sodium bicarbonate buffer.

The dendritic pattern, which can be generated by the diffusion-limited aggregation (DLA) of nanorods,[20] is an example of stochastic fractals. The fractal dimension, which is a measure of the structural complexity, is calculated to be 1.7 for the DLA of nanorods on a 2D surface.[20,37] Consistently, the fractal dimension for our peptide aggregates was estimated to be 1.68 to 1.79 by analyzing their SEM images on the basis of box counting, using the software of FracLac for ImageJ (Fig. S7†).[38] According to the model of DLA, the dendritic pattern was formed by the aggregation of the randomly moving nanorods through a touch-and-stick process on a 2D surface.[20]

Conformation of EASZ peptides

We had shown that the EASZ peptides could have three different aggregation states, *viz.*, amyloid fibrils, spaghetti-like bundles, and stochastic fractal under different conditions. If one could delineate the structural features characterizing each of these aggregation states, the driving force of the fractal forming process might be unraveled. To investigate the peptide conformation in solution, measurements of circular dichroism (CD) were carried out at different pH (Fig. 3). Accordingly, the peptides adopted largely a β-turn structure from pH 2.0 to 5.3, whereas the very low ellipticity above 210 nm and a negative band near 195 nm suggested that the peptides were in random-coiled conformation from pH 6.2 to 9.0.

To characterize the conformation of the aggregated peptides, solid-state NMR measurements were carried out. The sample of

 This journal is © The Royal Society of Chemistry 2020

Open Access Article. Published on 10 August 2020. Downloaded on 2/1/2026 3:57:00 AM.
This article is licensed under a Creative Commons Attribution-NonCommercial 3.0 Unported Licence.

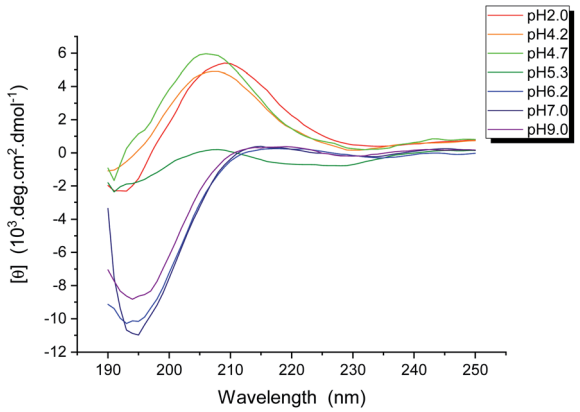

Fig. 3 CD spectra of the solution of EASZ peptides at different pH.

the fractal-forming peptides was uniformly ^{13}C enriched at Gly4, Ala5, and Glu12. The corresponding ^{13}C homonuclear correlation spectrum is shown in Fig. 4. Accordingly, the ^{13}C chemical shifts of Gly4, Ala5, and Glu12 were largely consistent with the β-sheet conformation. The full widths at half maximum ($\Delta\nu_{1/2}$) of Gly4 and Ala5 were *ca.* 2 ppm, which are the spectral feature of very well-structured amyloid fibrils.[39] The intensities of the cross peaks arising from Glu12 were in general weaker and broader than those from Gly4 and Ala5. The $\Delta\nu_{1/2}$ data of Glu12 were in the range of 2.5 to 3 ppm, revealing a moderate structural disorder at the C- and N-termini. Furthermore, the cross peak of Ala5-C^{α}/C^{β} appeared as a singlet for C^{α} and a doublet for C^{β}. This spectral feature strongly indicated the formation of steric zipper, where the methyl groups of Ala were either buried in the hydrophobic core or exposed to the solvent.[24,40,41] Steric zippers are formed by two peptide layers adopting the cross-β motif.[23] Thus, we concluded that the EASZ peptides adopted the β-sheet conformation in the fractal assembly. More importantly, the 2D spectrum revealed that the ^{13}C signals of the Ala, Gly, and Glu residues of EASZ peptides were well resolved so that $^{13}C\{^{1}H\}$ CPMAS of samples in natural abundance was sufficient to allow an unambiguous assignment.

The corresponding $^{13}C\{^{1}H\}$ CPMAS spectra for the peptides at three different aggregation states are shown in Fig. 5. The chemical shift data are summarized in Table S1.† Overall, the chemical shifts were approximately the same for the peptides at different aggregation states. The spectral signature of steric zipper was observed for all the samples. In other words, the peptides at the three aggregation states all adopted the cross-β motif. Nonetheless, the NMR signal intensities, which can be modulated by motional dynamics or structural heterogeneity, were significantly different for the three samples. For the Glu residues of the amyloid fibrils, only the C^{α} and C^{β} signals were observable. The absence of the sidechain signals of Glu were consistent with the expectation that the C- and N-termini of the EASZ peptides were highly disordered at low pH. That is, the structural order of the amyloid fibrils formed by EASZ under acidic conditions was mainly due to the close packing of the alanine-rich region. For the samples prepared under alkaline conditions, we found that the signal intensities of the Glu residues of the fractal-forming rods was higher than those of

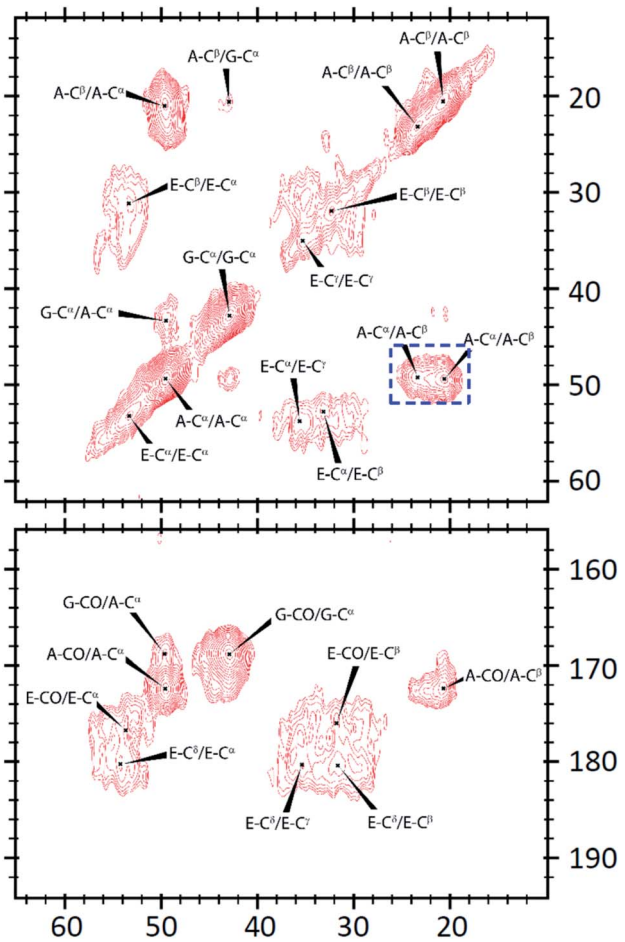

Fig. 4 Solid-state ^{13}C homonuclear correlation spectrum acquired for the EASZ peptides in fractal assembly. The spectral feature of steric zipper is highlighted by a dashed box in blue.

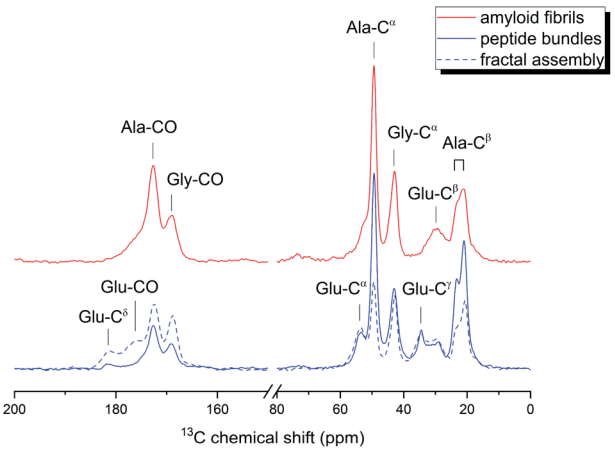

Fig. 5 $^{13}C\{^{1}H\}$ cross-polarization magic angle spinning spectra acquired for the EASZ peptides at different aggregation states. The samples were in natural abundance.

Open Access Article. Published on 10 August 2020. Downloaded on 2/1/2026 3:57:00 AM.
This article is licensed under a Creative Commons Attribution-NonCommercial 3.0 Unported Licence.

the peptide bundles. As a result, among the three aggregation states, the structural order at the Glu residues was the highest for the fractal assembly, intermediate for the peptide bundles, and lowest for the amyloid fibrils.

Conclusions

In summary, the EASZ peptides had exhibited a manifold of aggregation behaviors, *viz.* amyloid fibrils, peptide bundles, and fractal assembly, as a direct consequence of the interplay between the hydrophobic interaction and the ionic interaction among the peptide strands. Remarkably, the conformation of the peptides invariably adopted the motif of steric-zipper for all the three aggregation states. To obtain the fractal assembly for the EASZ peptides, the Glu residues had to be negatively charged. The structurally rigid and well dispersed nanorods would undergo random trajectory before they touched and stuck on a cluster, leading to the formation of a stochastic fractal assembly. Solid-state NMR is a useful technique in characterizing the subtle changes in peptide conformation at different aggregation states.

Conflicts of interest

There are no conflicts to declare.

Acknowledgements

This work was financially supported by the Ministry of Science and Technology, Taiwan (103-2113-M-002-013-MY3). The NMR, TEM, and SEM measurements were carried out at the Instrumentation Center of National Taiwan University, supported by the Ministry of Science and Technology. We thank C.-Y. Chien, S.-J. Ji, C.-Y. Lin, and Y.-Y. Yang for their help in TEM and SEM experiments.

Notes and references

1 B. B. Mandelbrot, *The fractal geometry of nature*, W. H. Freeman, San Francisco, 1982.
2 T. Vicsek, *Fractal Growth Phenomena*, World Scientific, Singapore, 2nd edn, 1992.
3 G. R. Newkome, P. Wang, C. N. Moorefield, T. J. Cho, P. P. Mohapatra, S. Li, S.-H. Hwang, O. Lukoyanova, L. Echegoyen, J. A. Palagallo, V. Iancu and S.-W. Hla, *Science*, 2006, **312**, 1782–1785.
4 M. Chen, J. Wang, S.-C. Wang, Z. Jiang, D. Liu, Q. Liu, H. Zhao, J. Yan, Y.-T. Chan and P. Wang, *J. Am. Chem. Soc.*, 2018, **140**, 12168–12174.
5 S.-Y. Wang, J.-Y. Huang, Y.-P. Liang, Y.-J. He, Y.-S. Chen, Y.-Y. Zhan, S. Hiraoka, Y.-H. Liu, S.-M. Peng and Y.-T. Chan, *Chem.–Eur. J.*, 2018, **24**, 9274–9284.
6 M. Yang and W. J. Song, *Nat. Commun.*, 2019, **10**, 5545.
7 J. Shang, Y. Wang, M. Chen, J. Dai, X. Zhou, J. Kuttner, G. Hilt, X. Shao, J. M. Gottfried and K. Wu, *Nat. Chem.*, 2015, **7**, 389–393.
8 G. Tikhomirov, P. Petersen and L. Qian, *Nature*, 2017, **552**, 67–71.
9 N. Chen, M. Zhao, C. Chassenieux and T. Nicolai, *Food Hydrocolloids*, 2016, **56**, 417–424.
10 R. Liu, Z. Kochovski, L. Li, Y. Yin, J. Yang, G. Yang, G. Tao, A. Xu, E. Zhang, H. Ding, Y. Lu, G. Chen and M. Jiang, *Angew. Chem., Int. Ed.*, 2020, **59**, 9617–9623.
11 S. Khatun, A. Singh, S. Maji, T. K. Maiti, N. Pawar and A. N. Gupta, *Soft Matter*, 2020, **16**, 3143–3153.
12 C. A. Machado, K. C. Bentz, R. Tran, T. A. Jenkins, B. E. Barnes, L. E. Diodati and D. A. Savin, *Biomacromolecules*, 2019, **20**, 2557–2566.
13 S. Shin, M.-L. Gu, C.-Y. Yu, J. Jeon, E. Lee and T.-L. Choi, *J. Am. Chem. Soc.*, 2018, **140**, 475–482.
14 N. Solodkov, J. Shim and J. C. Jones, *Nat. Commun.*, 2019, **10**, 198.
15 C. Cai, J. Lin, Y. Lu, Q. Zhang and L. Wang, *Chem. Soc. Rev.*, 2016, **45**, 5985–6012.
16 N. E. Hernández, W. A. Hansen, D. Zhu, M. E. Shea, M. Khalid, V. Manichev, M. Putnins, M. Chen, A. G. Dodge, L. Yang, I. Marrero-Berríos, M. Banal, P. Rechani, T. Gustafsson, L. C. Feldman, S.-H. Lee, L. P. Wackett, W. Dai and S. D. Khare, *Nat. Chem.*, 2019, **11**, 605.
17 Y. Georgalis, P. Umbach, J. Raptis and W. Saenger, *Acta Crystallogr., Sect. D: Biol. Crystallogr.*, 1997, **53**, 703–712.
18 A. Lomander, W. Hwang and S. Zhang, *Nano Lett.*, 2005, **5**, 1255–1260.
19 W. Shen, R. G. H. Lammertink, J. K. Sakata, J. A. Kornfield and D. A. Tirrell, *Macromolecules*, 2005, **38**, 3909–3916.
20 W. Wang and Y. Chau, *Soft Matter*, 2009, **5**, 4893–4898.
21 E. Mayans, G. Ballano, J. Casanovas, L. J. del Valle, M. M. Pérez-Madrigal, F. Estrany, A. I. Jiménez, J. Puiggalí, C. Cativiela and C. Alemán, *Soft Matter*, 2016, **12**, 5475–5488.
22 K. Giri, N. P. Bhattacharyya and S. Basak, *Biophys. J.*, 2007, **92**, 293–302.
23 M. R. Sawaya, S. Sambashivan, R. Nelson, M. I. Ivanova, S. A. Sievers, M. I. Apostol, M. J. Thompson, M. Balbirnie, J. J. W. Wiltzius, H. T. McFarlane, A. O. Madsen, C. Riekel and D. Eisenberg, *Nature*, 2007, **447**, 453–457.
24 H.-M. Cheng, T. W. T. Tsai, W. Y. C. Huang, H.-K. Lee, H.-Y. Lian, F.-C. Chou, Y. Mou and J. C. C. Chan, *Biochemistry*, 2011, **50**, 6815–6823.
25 D. S. Eisenberg and M. R. Sawaya, *Annu. Rev. Biochem.*, 2017, **86**, 69–95.
26 J. Schaefer and E. O. Stejskal, *J. Am. Chem. Soc.*, 1976, **98**, 1031–1032.
27 G. Metz, X. L. Wu and S. O. Smith, *J. Magn. Reson., Ser. A*, 1994, **110**, 219–227.
28 A. E. Bennett, C. M. Rienstra, M. Auger, K. V. Lakshmi and R. G. Griffin, *J. Chem. Phys.*, 1995, **103**, 6951–6958.
29 K. Takegoshi, S. Nakamura and T. Terao, *Chem. Phys. Lett.*, 2001, **344**, 631–637.
30 C. R. Morcombe, V. Gaponenko, R. A. Byrd and K. W. Zilm, *J. Am. Chem. Soc.*, 2004, **126**, 7196–7197.

 This journal is © The Royal Society of Chemistry 2020

Open Access Article. Published on 10 August 2020. Downloaded on 2/1/2026 3:57:00 AM.
This article is licensed under a Creative Commons Attribution-NonCommercial 3.0 Unported Licence.

31 R. R. Ernst, G. Bodenhausen and A. Wokaun, *Principles of Nuclear Magnetic Resonance in One and Two Dimensions*, Clarendon Press, Oxford, U.K., 1987.
32 D. Massiot, F. Fayon, M. Capron, I. King, S. Le Calve, B. Alonso, J. O. Durand, B. Bujoli, Z. H. Gan and G. Hoatson, *Magn. Reson. Chem.*, 2002, **40**, 70–76.
33 M. Biancalana, K. Makabe, A. Koide and S. Koide, *J. Mol. Biol.*, 2009, **385**, 1052–1063.
34 N. Yamada, K. Ariga, M. Naito, K. Matsubara and E. Koyama, *J. Am. Chem. Soc.*, 1998, **120**, 12192–12199.
35 N. J. Sinha, D. Wu, C. J. Kloxin, J. G. Saven, G. V. Jensen and D. J. Pochan, *Soft Matter*, 2019, **15**, 9858–9870.
36 T. A. Witten and L. M. Sander, *Phys. Rev. Lett.*, 1981, **47**, 1400–1403.
37 L. M. Sander, *Nature*, 1986, **322**, 789–793.
38 A. Karperien, *FracLac for ImageJ*, http://rsb.info.nih.gov/ij/plugins/fraclac/FLHelp/Introduction.htm, 1999.
39 A. T. Petkova, Y. Ishii, J. J. Balbach, O. N. Antzutkin, R. D. Leapman, F. Delaglio and R. Tycko, *Proc. Natl. Acad. Sci. U. S. A.*, 2002, **99**, 16742–16747.
40 S. W. Lee, Y. Mou, S.-Y. Lin, F.-C. Chou, W.-H. Tseng, C.-h. Chen, C.-Y. D. Lu, S. S.-F. Yu and J. C. C. Chan, *J. Mol. Biol.*, 2008, **378**, 1142–1154.
41 H.-M. Cheng, W. Y. C. Huang, T. W. T. Tsai, Y. Mou, J. C. H. Chao and J. C. C. Chan, *J. Chin. Chem. Soc.*, 2013, **60**, 794–800.